Polymer(Korea), Vol. 38, No. 4, pp. 449-456
http://dx.doi.org/10.7317/pk.2014.38.4.449

ISSN 0379-153X(Print)
ISSN 2234-8077(Online)

폴리락틱산, 폴리카프로락톤, 폴리에틸렌 옥사이드 삼성분계 블렌드의 형태학적 변화와 이들이 의료용 스캐폴더의 기계적 특성에 미치는 영향

Peyman Ezzati, Ismaeil Ghasemi†, Mohammad Karrabi, Hamed Azizi, and Ivan Fortelny*
Processing Faculty, Iran Polymer and Petrochemical Institute, *Institute of Macromolecular Chemistry AS CR
(2013년 12월 14일 접수, 2014년 2월 19일 수정, 2014년 3월 10일 채택)

Morphology Evolution of Poly(*L*-lactic acid) (PLLA), Poly(ε-caprolactone) (PCL) and Polyethylene Oxide (PEO) Ternary Blend and Their Effects on Mechanical Properties for Bio Scaffold Applications

Peyman Ezzati, Ismaeil Ghasemi†, Mohammad Karrabi, Hamed Azizi, and Ivan Fortelny*
Processing Faculty, Iran Polymer and Petrochemical Institute, PO Box 14965/115, Tehran, Iran
**Institute of Macromolecular Chemistry AS CR,Heyrovsky Sq. 2,162 06 Prague 6, Czech*
(Received December 14, 2013; Revised February 19, 2014; Accepted March 10, 2014)

Abstract: Ternary blends of poly(*L*-lactic acid) (PLLA), poly(ε-caprolactone) (PCL) and polyethylene oxide (PEO) were produced with different concentrations of components via melt blending. By leaching the PEO from the samples by water, porous materials were obtained with potential application for bio scaffolds. Sample porosity was evaluated by calculating the ratio of porous scaffold density (ρ^*) to the non-porous material density (ρ_s). Highest porosity (51.42%) was related to the samples containing 50 wt%. of PEO. Scanning electron microscopy (SEM) studies showed the best porosity resulted by decreasing PLLA/PCL ratio at constant concentration of PEO. Crystallization behavior of the ternary blend samples was studied using differential scanning calorimetry (DSC). Results revealed that the crystallinity of PLLA was improved by addition of PEO and PCL to the samples. The porosity plays a key role in governing the compression properties. Mechanical properties are presented by Gibson-Ashby model.

Keywords: PLLA/PCL/PEO ternary blend, bio scaffold, melt blending, morphology, porosity.

Introduction

Polymer blending is one of the most fascinating and rapidly growing areas in polymer science and technology and an effective way to develop new materials with higher performance.[1,2] Melt blending of two or more polymers is a collaborative approach to develop new material with customized properties.[3,4]

Prediction, control and study of morphology and mechanical properties in polymer blend especially in ternary polymer blend are a difficult task.[5,6] Generally the morphology of a ternary polymer blend is depended on interaction parameters among three components, rheological properties of the components and processing conditions.[7,8]

From a thermodynamic viewpoint, ternary blends of homo polymers A, B, and C can typically display four types of morphologies, as predicted by the minimizing of the interfacial free energy. Three of them are complete wetting types of morphology, where one of the polymers forms a layer at the interface of the two others that can be seen in Figure 1(a) to (c). The fourth microstructure corresponds to partial wetting which is characterized by a line of 3-phase contact between the materials shown in Figure 1(d). As demonstrated by Torza and Mason,[9-11] each of these morphologies is characterized by a set of three spreading coefficients λ_{ijk} that are functions of the interfacial tensions between the materials.

Investigation of ternary polymer blends was first reported in the 1980s by Hobbs *et al*.[3,12,13] In particular, they used the concept of spreading coefficient and rewrote Harkin's equation in which two distinct phases are dispersed in a matrix phase to predict the morphology of ternary blends. In a ternary blend of

†To whom correspondence should be addressed.
E-mail: i.ghasemi@ippi.ac.ir

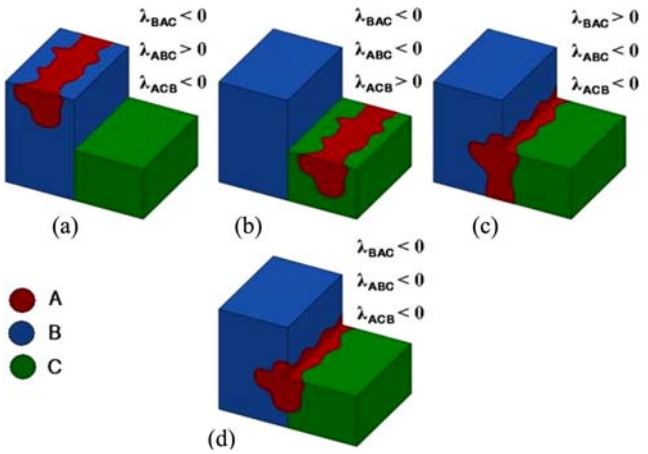

Figure 1. Morphologies in ternary polymer blend comprised of two major phases B and C and minor phase A as predicted by spreading coefficient (λ). (a) to (c); complete wetting; (d) partial wetting.

three polymers A, B, and C, the spreading coefficient, λ_{ijk}, can be defined as eq. (1) to (3).[4,12,13]

$$\lambda_{BAC} = \gamma_{BC} - (\gamma_{AB} + \gamma_{AC}) \quad (1)$$

$$\lambda_{ABC} = \gamma_{AC} - (\gamma_{AB} + \gamma_{BC}) \quad (2)$$

$$\lambda_{ACB} = \gamma_{AB} - (\gamma_{AC} + \gamma_{BC}) \quad (3)$$

Where, γ_{ij} is the interfacial tension between the polymers. Using the harmonic mean equation which is written in eq. (4).[4,12,13]

$$\gamma_{ij} = \gamma_i + \gamma_j - \frac{4\gamma_i^d \gamma_j^d}{\gamma_i^d + \gamma_j^d} - \frac{4\gamma_i^p \gamma_j^p}{\gamma_i^p + \gamma_j^p} \quad (4)$$

Where γ_i is the surface tension of component *i*; γ_i^d is the dispersive fraction of the surface tension of component *i* and γ_i^p is the polar fraction of the surface tension of component *i*.

Much less work has been carried out on the fundamental morphological states occuring in ternary polymer blends.[14]

A number of morphologies in ternary high-density polyethylene (HDPE)/polystyrene (PS)/poly(methyl methacrylate) (PMMA) blends have been surveyed. Reignier *et al.*[15] examined the core-shell morphology of PMMA encapsulated by PS in an HDPE matrix in detail. Zhang *et al.*[16] studied PS/PMMA/polycarbonate (PC) systems, where complete wetting was observed as predicted by the theory. Omonov *et al.*[17] found morphology containing several types of structure in polyamide (PA)/polypropylene (PP)/PS blends with PA matrix-PP particles fully or partly encapsulated with PS simultaneously with isolated PS particles was detected. Guo *et al.*[18,19] studied the morphology of ternary and quaternary blends and proposed a model which includes not only the interfacial tension, but also the interfacial area of the phases. To date, however, the detailed examination of all the possible morphological states over the entire composition range for a ternary polymer blend has not been carried out. Koseki *et al.*[20] found that type of the morphology formed at mixing can change during annealing. Reignier *et al.*[21] showed that substitution of γ_{ij} improved the agreement with experimental data.

Thermoplastic aliphatic polyesters such as, polyglycolide, polycaprolactone, polylactide and their blends have generated interest because of their excellent biocompatibility, biodegradability, and mechanical strength.[22,23] Poly(*L*-lactic acid) (PLLA) is a poly(a-hydroxy acid) and poly(ε-caprolactone) (PCL) is a poly(x-hydroxy acid) and both of them are biocompatible and biodegradable.[24,25] PLLA is a rigid, transparent and semi-crystalline polymer.[24,25] On the other hand, PCL can be used as a polymeric plasticizer because of its ability to lower elastic modulus and to impact modifier of other polymers.[24-26] Polyethylene oxide (PEO) is also biodegradable and biocompatible polymer which can be easily dissolved in water.[24-26] PLLA/PCL blends have attracted great interest as temporary absorbable implants in the human body, but they suffer from poor mechanical properties due to macro phase separation of the two immiscible components and to poor adhesion between phases.[25-27] PLLA is mixed with a ductile biodegradable polymer such as PCL having much lower strength and modulus than PLLA.[22]

The mechanical properties of PLLA/PCL blends have been characterized in the previous studies;[22,26] however, few studies have been performed on the development and characterization of porous structures of PLLA/PCL.[28]

Porous foams of biodegradable polymers have received much attention in biomedical applications and melt blending has recently been reported as a versatile protocol for processing porous materials.[28-30] The foams are used as bio scaffolds and membranes for tissue engineering and support materials of drug delivery systems.[31,32] It is therefore important to develop bio scaffolds having a wide range of mechanical properties by controlling their structures and constituents.[33,34]

In this study, porous PLLA/PCL was fabricated by PLLA/PCL/PEO melt blending in internal mixer and then extracting PEO part by water to produce porous PLLA/PCL. The main objective of this work is to contribute to this topic by studying

the effects of concentrations of blend component on the porosity, compressive mechanical properties, thermal properties and morphologies of porous PLLA/PCL blends.

Experimental

Materials. PCL and PEO were obtained from Sigma-Aldrich. PLLA was purchased from Nature Works LLC. Number average molecular weight (M_n), glass transition temperature (T_g), melting temperature (T_m) and density of the polymers are reported in Table 1.

Sample Preparation. Ternary blends were prepared by melt mixing in a Haake internal mixer with Banbury blades. The mixing blades were maintained at 60 rpm and the temperature was set at 190 °C. PLLA and PCL dry mixed and then fed into the mixing chamber. After melting of PLLA/PCL dried, PEO was added and mixing was continued up to 10 min. The blends were then quenched under liquid nitrogen to freeze in the morphology. The compositions and sample codes are presented in Table 2.

Morphology Observation. A scanning electron microscope (SEM), Tescan VEGA-II SEM, was used to examine the samples morphology. The PLLA/PCL/PEO were fractured in liquid nitrogen and leached with deionized water for 7 days at ambient temperature to selectively extract the PEO water soluble component. The cross-sections were coated with platinum using a sputter coater (Emitech K575X) operating at 10 mA for about 15 s under argon atmosphere.

Table 1. Characteristics of Polymers

Materials	$M_n \times 10^{-3}$ (g/mol)[a]	T_g (°C)[a]	T_m (°C)[a]	Density (g/cm^3)
PCL	70-90 by GPC	-69	60	1.14
PEO	100	-67	65	1.13
PLLA	-	61	190	1.24

[a]Obtained from suppliers.

Table 2. Compositions of Polymer Components

Sample code	PLLA (wt%)	PEO (wt%)	PCL (wt%)
CEL 1	30	10	60
CEL 2	40	20	40
CEL 3	40	30	30
CEL 4	10	80	10
CEL 5	10	40	50
CEL 6	25	25	50
CEL 7	60	10	30
CEL 8	30	30	40
CEL 9	50	40	10
CEL 10	10	50	40
CEL 11	25	50	25
CEL 12	40	50	10

Measurement of the Interfacial Tensions. PLLA/PCL, PLLA/PEO and PCL/PEO interfacial tensions were measured at room temperature using sessile drop method on Kruss G10, Germany. PLLA, PCL and PEO films of thickness averaging 200 microns were made by compression molding.

Solvent Extraction and Continuity of the Porogen Phase. Selective solvent extractions of PEO in deionnized water were performed for 7 days at room temperature over the whole composition range. Weight-loss measurements were carried out to evaluate the extent of PEO continuity using the eq. (5):[28,33,34]

$$\%\text{PEO Contiuity} = \left(\frac{\text{weight PEO}_{\text{initial}} - \text{weight PEO}_{\text{final}}}{\text{weight PEO}_{\text{initial}}}\right) \times 100 \quad (5)$$

Using the PEO continuity, the pore-to-volume ratio of the porous PLLA/PCL blend is directly evaluated (the variation of the densities between melting and room temperature leads to an error of 0.02 on the percentage of pore-to-volume ratio).[35]

Porosity Measurement. Assuming that porogen PEO phase are completely extracted out due to the co-continuous morphology of the PLLA/PCL blends, the porosity or void volume fraction V_f (%) of the porous PLLA/PCL blends was calculated using the eq. (6):[35-37]

$$V_f = \left(1 - \frac{\rho^*}{\rho_s}\right) \times 100 \quad (6)$$

Where ρ^* is the apparent density of the porous scaffold and ρ_s is the density of the non-porous material or skeletal density.

Thermal Properties. Differential scanning calorimetric (DSC) measurements were carried out under nitrogen atmosphere using NETZCH, 200 F3. The samples of about 15-20 mg were dried in a vacuum oven before the experiment. The heating-cooling-heating cycles were recorded in the temperature range from 0 to 200 °C at a scan rate of 10 °C/min under nitrogen atmosphere. In the first heating run, all the samples were annealed at the final temperature (200 °C) for 3-4 min to delete the previous thermal history.

The melting temperature (T_m), crystallization temperature (T_c), and glass transition temperature (T_g) of both virgin and

blended samples were determined. The intrinsic degree of crystallinity, X_c, was determined based on:[38,39]

$$\%X_i = \frac{\Delta H_{fs_i}}{W \times \Delta H_{f100\%_i}} \quad (7)$$

Where ΔH_{fs_i} designate the measured enthalpy of melting, and and $\Delta H_{f100\%_i}$ represents the enthalpy for 100% crystalline for polymer *i*.

Compressive Mechanical Test. Compressive mechanical properties were measured at room temperature on an SANTAM STM-20 equipped with a 500 kgf load. The crosshead speed was kept at a value of 1 mm/min. Cylindrical specimens with diameter: 12 mm and height: 10 mm, were fabricated using a circular mold in compression molding at 190 ºC. The reported values are the average of three tests for each sample.

Results and Discussion

Morphology. In order to predict the formed morphology of PLLA/PCL/PEO ternary blend during melt blending, spreading coefficients were determined. At first, interfacial tensions of the components were measured at room temperature and then extrapolated to the processing temperature (190 ºC). When plotting surface tension (γ) versus temperature (T), straight lines are obtained for a considerable number of polymers.[38,40] The change in surface tension ($-d\gamma/dT$) is 0.1 mN/m per degree for small molecules. For polymers the value is lower, that is 0.05 mN/m per degree.[39,41]

Spreading coefficient was calculated according to eq. (1) to (4) and depicted in Table 3. Considering two negative and one positive spreading coefficient, it is clear that the complete wetting was obtained. In other words, the typical morphology were formed which is illustrated in Figure 1(a) to (c).

SEM micrographs of the samples containing different concentration of the PEO are shown in Figure 2(a) to (f). In this figure the black holes corresponds to extracted PEO by water. As seen in the whole range of PEO concentration, the complete wetting occurred and the porosity was created by leaching the PEO. However, due to low concentration values that are given in Table 4 of PEO, the low porosity is expected in sample CEL 1 as shown in Figure 2(a).

With increase in PEO content of the samples, the porosity increased which is depicted in Table 4. The highest porosity which is suitable for tissue engineering was related to sample CEL 11 (51.42%) with 50 wt% PEO content that shown in Figure 2(e). Our results showed that above 50 wt% of PEO there is no framework of porous PLLA/PCL blend and it is not suitable for using in bio scaffold application (Figure 2(f)). Figure 3 shows the continuity of PEO phase in the samples versus PEO content. It is obvious that the full continuity is at 50 wt% concentration of PEO. In other words, assessing a framework with appropriate dimensional stability is impossible over 50 wt% of PEO that is shown with the dashed line in this figure. It seems, the morphology of obtained highest porosity was shown in Figure 2(e) obeys from pattern of Figure 1(a) and (b).

Table 3. Surface Tension, Interfacial Tensions and Spreading Coefficients of Neat and Blend Samples

Surface tension @ 25 ºC (mN/m)		
γ_{PLLA}^{d}=43.10	γ_{PLLA}^{p}=30.47	γ_{PLLA}=73.57
γ_{PCL}^{d}=45.82	γ_{PCL}^{p}=5.79	γ_{PCL}=51.61
γ_{PEO}^{d}=45.60	γ_{PEO}^{p}=22.83	γ_{PEO}=68.42
$\gamma_{PLLA/PCL}$=16.90	$\gamma_{PLLA/PEO}$=1.16	$\gamma_{PEO/PCL}$=10.14
Interfacial tensions @ 190 ºC (mN/m)		
γ_{PLLA}^{d}=34.56	γ_{PLLA}^{p}=17.95	γ_{PLLA}=60.76
γ_{PCL}^{d}=37.45	γ_{PCL}^{p}=-6.87	γ_{PCL}=38.83
γ_{PEO}^{d}=37.12	γ_{PEO}^{p}=8.87	γ_{PEO}=54.34
$\gamma_{PLLA/PCL}$=72.21	$\gamma_{PLLA/PEO}$=19.68	$\gamma_{PEO/PCL}$=140.38
Spreading coefficient (mN/m) of ternary		
$\lambda_{PCL/PLLA/PEO}$= 48.48		Positive
$\lambda_{PLLA/PCL/PEO}$= -192.92		Negative
$\lambda_{PLLA/PEO/PCL}$= -87.58		Negative

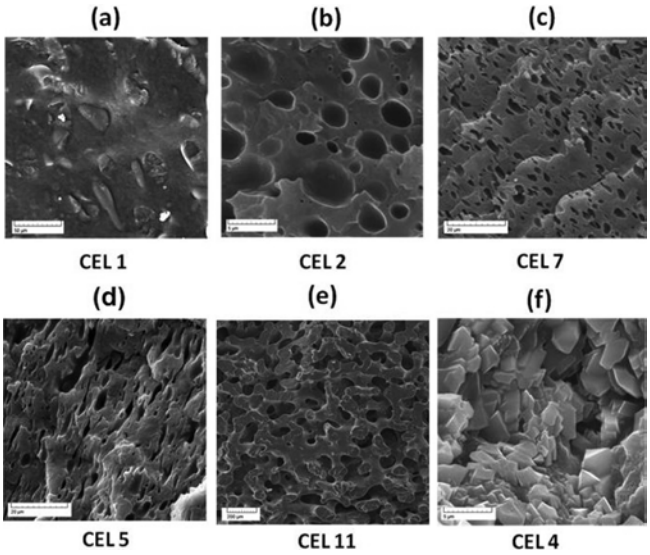

Figure 2. SEM micrograph of PLLA/PCL/PEO blends in different PEO concentrations: (a) 10 wt%; (b) 20 wt%; (c) 30 wt%; (d) 40 wt%; (e) 50 wt%; (f) 80 wt% of PEO.

Table 4. Sample Porosity and PEO Continuity

Sample	CEL 1	CEL 2	CEL 4	CEL 5	CEL 7	CEL 10	CEL 11	CEL 12
V_f (%)	8.16	17.31	0.00	3.68	26.82	40.53	51.42	40.68
PEO Continuity (%)	16.75	37.45	0.00	91.54	41.67	91.36	91.84	86.94

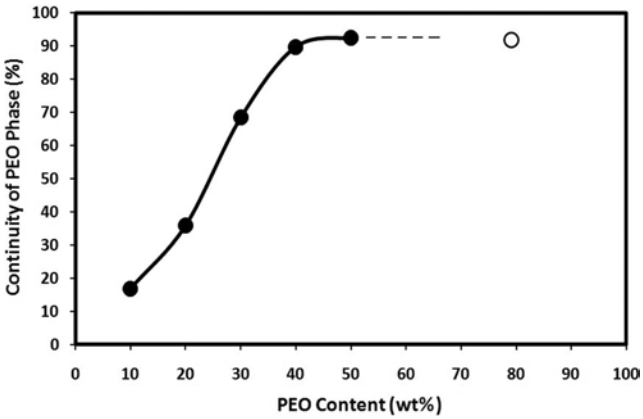

Figure 3. PEO phase continuity as a function of PEO content. The white circle indicates the concentration at which there is no framework.

On the other hand, compressive behavior in porous material and bio scaffold application is important so that this property for our samples should be considered. For this reason the PLLA/PCL ratios in the samples containing highest porosity were changed. SEM micrographs and schematic morphology of these samples with 50 wt%. PEO and different PLLA/PCL ratio (10/40, 25/25, and 40/10 wt%) are demonstrated in Figure 4.

The onset of disintegration above 50 wt% of PEO the porous PLLA/PCL network loses some part of its mechanical integrity and begins to collapse. In Figure 4 the white borders of the porous may be attributed to the PLLA phase due to higher crystallization percent. Location of the PLLA at the porous border may also be related to lower interfacial tension of $\gamma_{PLLA/PEO}$: 19.68 mN/m in comparison to $\gamma_{PCL/PEO}$: 140.38 mN/m and $\gamma_{PLLA/PCL}$: 72.21 mN/m. In other words, as schematically shown in Figure 4(b), (d) and (f) interfacial surface between PCL and PEO was not formed.

By increasing PLLA concentration in PLLA/PCL constant concentration (50 wt%) in PLLA/PCL/PEO blend samples, formation of droplet-matrix morphology is expected while the PCL is dispersed PLLA matrix as shown in Figure 4(e) and (f).

Crystallization. Since the mechanical properties of the blends are strongly affected by crystallization, this phenomenon was studied. Analysis of crystallization behavior of ternary blend is complex and there are a few reports in this field. This PLLA/PCL/PEO ternary blend seems to be a complicated one for analysis by DSC because its three components are all crystalline. The cooling step of DSC thermograms and the relevant DSC data are demonstrated in Figure 5 and Table 5 respectively for pure components and ternary blend samples respectively.

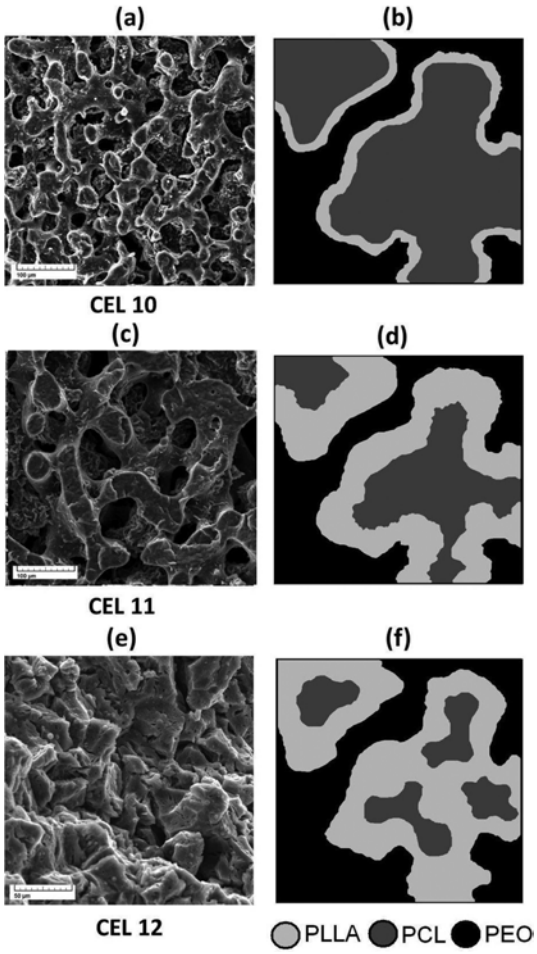

Figure 4. SEM micrographs of samples in 50 wt% of PEO with PLLA/PCL blends ratio (a) 10/40; (c) 25/25; (e) 40/10. (b); (d); (f) schematic representation of (a), (b), and (c), respectively. Note that in all schematics black, gray and white represents the PEO, PCL and PLLA phases, respectively.

As seen there is no crystallization peak in pure PLLA which implies low rate of crystallization for this polymer. By addition

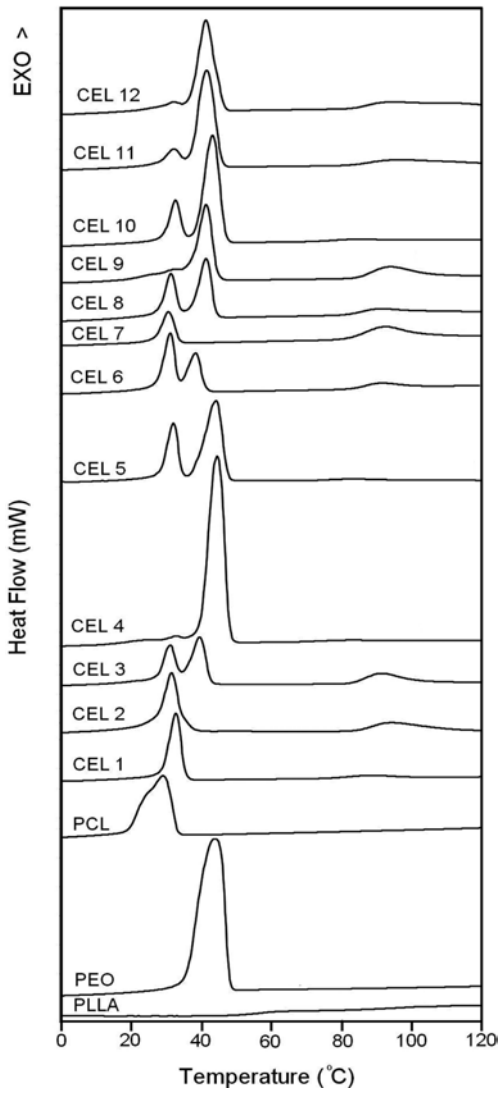

Figure 5. DSC thermograms in reheating step for pure components and the PLLA/PCL/PEO blend samples scaned at 10 °C/min.

of other components crystallization peak was observed in DSC thermogram which means PLLA crystallization was improved. In other words in applied condition test (10 °C/min) the crystalline cells of pure PLLA cannot be formed. It seems that the main reason for this phenomenon is the formation of a strong interface between PLLA and PEO because of the better compatibility[42] in comparison to PLLA and PCL phases.[43]

It seems PEO chains can be regarded as a defect during the PLLA crystallization which leads to more efficient nucleation, in the case of polymer blend diffusion of solutes, viscous flows in the melt, solid-liquid interface growth and motion, and, finally, formation of non-equilibrium crystalline defects generated within the solid phase as a crystal grows rapidly.[44-46]

Another effect of the existence of PCL and PEO on the PLLA crystallization is the elimination of cold crystallization. The cold crystallization in PLLA is originated from the incomplete crystalline structure due to its low crystallization rate. As mentioned above as a result of addition of PCL and PEO into PLLA, crystallization was improved and the perfect crystals less or more were formed.

Because of remaining PCL in the porous samples after PEO leaching, studying crystallization of PCL is necessary. As seen in Table 5 the crystallization temperature peak and percent of crystallization of PCL were increased because presence of solid PLLA in the temperature range of PCL crystallization (30 to 40 °C) induces heterogeneous nucleation for the formation of PCL crystals. Enhancement of PCL crystallization can be also observed in higher crystallization temperature (T_c) of samples. Generally, our results in this section showed that more and fast crystallization were monitored for PCL and PLLA as the main structure of the porous material.

Mechanical Properties. The most common test for mechanical evaluation of porous materials especially bio scaffold is evaluating the compressive properties. In this study, the compression behavior is affected by the amount of porosity, ratio of PLLA/PCL in porous scaffold and crystallinity. Table 6 reports porosity, apparent, non-porous scaffold density and the compression modulus in linear elasticity zone of compressive test that is typically strain less than 3%.

Regarding our results, it seems the porosity plays the main role in controlling of compressive modulus of samples. As seen from Table 6, with increasing porosity, the compressive modulus decreases. The lowest modulus is related to samples CEL 11 due to the highest porosity.

For more explanation of compressive behavior, the Gibson-Ashby model that is shown in eq. (8) can be used.[35] Based on this model the compressive modulus (E^*) is given as a power law trend:

$$E^* = c\left(\frac{\rho^*}{\rho_s}\right)^m \quad (8)$$

Where c is the compression modulus of the non-porous material, whereas m is the power-law exponent which should vary between 1 and 2 for isotropic open-cell foam with uniformly distributed cells.[35] On a log-log plot, the relationship between compressive modulus and the relative density follows a power-law as expected from the deformation mechanisms of foams model proposed by Gibson and Ashby. Our data were fitted to Gibson-Ashby model and shown in Figure 6. The

Table 5. DSC Data of PLLA/PCL/PEO Ternary Blends

	T_{mPCL} (°C)	T_{mPEO} (°C)	T_{mPLLA} (°C)	T_{cPCL} (°C)	T_{cPEO} (°C)	T_{cPLLA} (°C)	ΔH_{cPCL} (J/g)	ΔH_{cPEO} (J/g)	ΔH_{cPLLA} (J/g)	$\%X_{PCL}$	$\%X_{PEO}$	$\%X_{PLLA}$
PCL	56.56	-	-	28.98	-	-	-56.56	-	-	39.67	-	-
PEO	-	67.14	-	-	43.67	-	-	-135.22	-	-	71.21	-
PLLA	-	-	170.83	-	-	-	-	-	-	-	-	42.51
CEL 1	56.18	-	167.34	32.73	-	87.8	33.71	-	3.67	44.06	-	52.93
CEL 2	56.31	-	168.00	31.54	-	93.85	40.99	-	15.08	77.67	-	57.36
CEL 3	56.98	60.41	168.19	31.12	39.51	91.2	26.09	21.85	15.09	62.25	44.87	61.81
CEL 4	56.8	61.8	160.48	32.79	44.36	-	9.53	102.63	-	89.78	64.89	46.35
CEL 5	56.57	62.65	163.41	32.05	44.03	82.14	28.92	49.76	2	66.97	48.26	54.94
CEL 6	57.56	60.92	168.39	31.3	38.71	91.6	29.94	18.49	6.51	46.77	33.71	55.44
CEL 7	56.97	-	169.23	30.7	-	92.01	16.34	-	19.99	28.78	20.71	48.5
CEL 8	57.56	62.38	168.62	31.43	41.35	90.62	22.79	28.83	8.62	54.57	39.34	57.02
CEL 9	56.3	61.46	167.29	32.45	41.28	93.51	12	41.84	17.05	44.45	32.41	55.03
CEL 10	57.08	62.69	163.35	32.59	43.08	83.43	22.08	59.17	2.45	66.83	48.17	57.63
CEL 11	57.54	62.23	165.63	32.13	41.51	95.95	12.84	56.98	10.90	68.76	49.56	59.95
CEL 12	57.57	63.11	167.41	32.26	41.33	93.46	7.96	54.16	14.59	76.05	55.33	54.54

Table 6. Compressive Modulus, Porosity, Bulk Density (d^*), and Skeletal Density (d_s) of Porous PLLA/PCL

Sample	Com. modulus (KPa)	V_f (%)	d^* (g/cm^3)	d_s (g/cm^3)	Relative density
CEL 1	640	8.16	1.03	1.12	0.92
CEL 2	160	17.3	0.99	1.12	0.89
CEL 3	150	19.9	0.9	1.14	0.79
CEL 5	270	30.7	0.78	1.13	0.69
CEL 6	720	25.23	0.85	1.13	0.75
CEL 7	1580	4.63	1.1	1.13	0.97
CEL 8	830	34.57	0.75	1.15	0.65
CEL 9	210	41.97	0.68	1.17	0.58
CEL 10	190	40.53	0.67	1.13	0.56
CEL 11	70	51.42	0.55	1.14	0.48
CEL 12	90	40.68	0.7	1.17	0.59

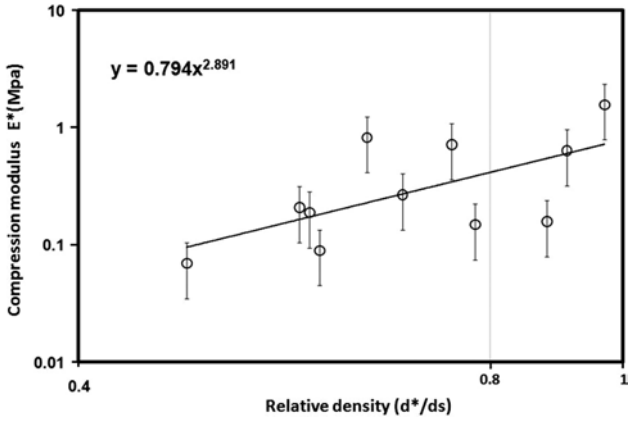

Figure 6. Compressive modulus of PLLA/PCL porous scaffolds as a function of relative density.

power law exponent was m=2.89. This value is valid over the porosity range of the data 8-52% which is a high in comparison to theoretical range of uniform isotropic open cells. Similar observations have been reported for other scaffold materials.[35]

The higher value of m in this work implies more dependency of compressive modulus to porosity. In other words, the sensitivity of the modulus to the porosity in our samples is more pronounced. Nevertheless, the dependence of compression modulus on porosity or relative density, which is specific to the material and fabrication methods, provides the opportunity to tailoring the biomechanical response of the scaffold to the damaged tissue.

Conclusions

The analysis of ternary blend properties based on PLLA, PCL and PEO and evaluation of its potential for using in bio scaffold were discussed. The porous material was obtained by leaching of PEO from samples using water. The following conclusions were drawn from the morphological, crystallinity and compressive properties studies.

1. The complete wetting morphology is predicted by Harkins equations and confirmed by SEM micrographs.

2. The rate and amount of crystalline of PLLA are improved by addition of PCL and PEO in the samples and cold crystallization of PLLA disappeared in the second heating.

3. The highest porosity (51.42%) is obtained from the samples contain 50 wt% of PEO and PLLA/PCL with 25 wt%/25 wt%.

4. At the constant concentration of PEO (50 wt%) and decrease of PLLA/PCL ratio, the best properties is obtained by decreasing the PLLA/PCL ratio.

5. Compressive modulus of the samples is affected by degree of porosity, ratio of PLLA/PCL in porous scaffold and its crystallinity. The porosity, however, plays the main role in variation of compression modulus.

References

1. I. Fortelný, J. Juza, and B. Dimzoski, *Eur. Polym. J.*, **48**, 1230 (2012).
2. P. Ezzati, I. Ghasemi, M. Karrabi, and H. Azizi, *Iran Polym. J.*, **17**, 265 (2008).
3. S. H. Shokoohi and A. Arefazar, *Polym. Adv. Technol.*, **20**, 433 (2009).
4. P. Sarazin, G. Li, W. J. Orts, and B. D. Favis, *Polymer*, **49**, 599 (2008).
5. I. Fortelny, M. Lapcikova, J. Mikesova, and J. Juza, *J. Polym. Sci., Part B: Polym. Phys.*, **47**, 2158 (2009).
6. N. Virgilio, P. Desjardins, G. L'Esperance, and B. D. Favis, *Polymer*, **51**, 1472 (2010).
7. K. H. A. Aamer, H. Sardinha, and S. R. Bhatia, *Biomaterials*, **25**, 1087 (2004).
8. I. Luzinov, C. Pagnoulle, and R. Jerome, *Polymer*, **41**, 3381 (2000).
9. S. Torza and S. G. Mason, *J. Colloid Interface Sci.*, **33**, 67 (1970).
10. N. Virgilio, P. Sarazin, and B. D. Favis, *Biomaterials*, **31**, 5719 (2010).
11. P. Le Corroller and B. D. Favis, *Polymer*, **52**, 3827 (2011).
12. S. Ravati and B. D. Favis, *Polymer*, **52**, 718 (2011).
13. S. Y. Hobbs, M. E. J. Dekkers, and V. H. Watkins, *Polymer*, **29**, 1598 (1988).
14. S. Ravati and B. D. Favis, *Polymer*, **51**, 4547 (2010).
15. J. Reignier and B. D. Favis, *Macromolecules*, **33**, 6998 (2000).
16. J. Zhang, S. Ravati, N. Virgilio, and B. D. Favis, *Macromolecules*, **40**, 8817 (2007).
17. T. S. Omonov, C. Harrats, and G. Groeninckx, *Polymer*, **46**, 12322 (2005).
18. H. F. Guo, N. V. Gvozdic, and D. J. Meier, *Polymer*, **38**, 4915 (1997).
19. H. F. Guo, S. Packirisamy, N. V. Gvozdic, and D. J. Meier, *Polymer*, **38**, 785 (1997).
20. Y. Koseki, M. S. Lee, and C. W. Macosko, *Rubber Chem. Technol.*, **72**, 109 (1998).
21. J. Reignier, B. D. Favis, and M. C. Heuzey, *Polymer*, **44**, 49 (2003).
22. G. Maglio, M. Malinconico, A. Migliozzi, and G. Groeninckx, *Macromol. Chem. Phys.*, **205**, 946 (2004).
23. B. Dhandayuthapani, Y. Yoshida, T. Maekawa, and D. S. Kumar, *Int. J. Polym. Sci.*, **1**, 1 (2011).
24. W. Y. Ahn, H. L. Kim, J. E. Song, D. Lee, and G. Khang, *Polymer(Korea)*, **35**, 499 (2011).
25. A. Y. Oh, S. H. Kim, S. J. Lee, J. J. Yoo, M. van Dyke, J. M. Rhee, and G. Khang, *Polymer(Korea)*, **32**, 403 (2008).
26. Y. Kodama, L. D. B. Machado, C. Giovedi, and K. Nakayama, *Nucle. Instrum. Method. Phys. Res. B*, **265**, 294 (2007).
27. R. D. Erba, G. Groeninckx, G. Maglio, M. Malinconico, and A. Migliozzi, *Polymer*, **42**, 7831 (2001).
28. M. Todo, J. E. Park, H. Kuraoka, J. W. Kim, K. Taki, and M. Ohshima, *J. Mater. Sci.*, **44**, 4191 (2009).
29. M. Todo, S. D. Park, T. Takayama, and K. Arakawa, *Eng. Fract. Mech.*, **74**, 1872 (2007).
30. W. Zhang, D. Yao, Q. Zhang, J. Zhou, and P. Lelkes, *Biofabrication*, **2**, 1 (2010).
31. T. Tanaka, S. Eguchi, H. Saitoha, M. Taniguchi, and D. R. Lloyd, *Desalination*, **234**, 175 (2008).
32. A. J. Salgado, O. P. Coutinho, and R. L. Reis, *Macromol. Biosci.*, **4**, 743 (2004).
33. H. R. I. Khasim, S. Henning, G. H. Michler, and J. Brand, *Macromol. Symp.*, **294**, 144 (2010).
34. A. G. Mikos and J. S. Temenoff, *Electron. J. Biotechnol.*, **3**, 1 (2000).
35. J. Reignier and M. A. Huneault., *Polymer*, **47**, 4703 (2006).
36. P. Sarazin, X. Roy, and B. D. Favis, *Biomaterials*, **25**, 5965 (2004).
37. M. H. Hoa, P. Y. Kuoa, H. J. Hsieha, T. Y. Hsienb, L. T. Houc, J. Y. Laid, and D. M. Wang, *Biomaterials*, **25**, 129 (2004).
38. H. Tsuji, G. Horikawa, and S. H. Itsuno, *J. Appl. Polym. Sci.*, **104**, 831 (2007).
39. D. Pinoit and R. E. Prudhomme, *Polymer*, **43**, 2121 (2003).
40. S. Gomari, I. Ghasemi, M. Karrabi, and H. Azizi, *J. Polym. Res.*, **19**, 1 (2012).
41. M. Lewin, A. M. Marom, and R. Frank, *Polym. Adv. Technol.*, **16**, 429 (2005).
42. A. J. Nijenhuis, E. Colstee, D. W. Grijpma, and A. J. Pennings, *Polymer*, **37**, 5849 (1996).
43. Sh. W. Kuo, Ch. F. Huang, Y. Ch. Tung, and F. Ch. Chang, *J. Appl. Polym. Sci.*, **100**, 1146 (2006).
44. T. Jurkin and I. Pucic, *Radiat. Phys. Chem.*, **81**, 1303 (2012).
45. V. Ojijo, Th. Malwela, S. S. Ray, and R. Sadiku, *Polymer*, **53**, 505 (2012).
46. M. Wang, *Am. J. Biochem. Biotechnol.*, **2**, 80 (2006).